Transient Stability-Constrained Optimal Power Flow Calculation with Extremely Unstable Conditions using Energy Sensitivity Method

Shiwei Xia, *Senior Member, IEEE,* Zhaohao Ding, Mohammad Shahidehpour, *Fellow, IEEE,* Ka Wing Chan, Siqi Bu, *Senior Member, IEEE,* Gengyin Li

Abstract: **In this paper, a transient stability margin is proposed in terms of the kinetic energy of power systems in extremely unstable conditions. A unified energy-based transient stability constraint is formed for both normal and extremely unstable conditions in the proposed transient stability-constrained optimal power flow (TSCOPF) model. A divide-and-conquer approach is presented to solve TSCOPF by decomposing it into optimal power flow and transient stability constraint formation subproblems. The former is solved by an interior point method and the latter is derived by an energy sensitivity technique. Furthermore, an accuracy-based perturbation strategy is proposed to address the system over-stabilization issue, and a parallel calculation technique is implemented to speed up the TSCOPF solution. The effectiveness of the proposed approach is investigated and the results are validated using the New England 10-generator and IEEE 50-generator systems under extremely unstable conditions.**

***Index Terms*: Optimal power flow, transient stability, energy sensitivity, extremely unstable condition, accuracy-based perturbation strategy.**

I. Introduction

The transient stability-constrained optimal power flow (TSCOPF) problem, which offers a compromise between economic and secure operations of power systems, has attracted much attention recently. TSCOPF is a time-consuming semi-infinite optimization problem for preventive control which considers differential-algebraic equations (DAEs) for describing system dynamics and transient stability constraints [1]. Presently, three methods for solving TSCOPF are available which include generation rescheduling, numerical discretization, and artificial intelligence (AI) algorithms.

Generation rescheduling shifts power system generation from unstable region into stable region in order to find a solution for TSCOPF. In [2],[3], the time-domain simulation and generation reschedule procedures were iteratively conducted for solving TSCOPF. In [4], a novel divide-and-conquer approach was presented by decomposing the original TSCOPF into a master optimal power flow (OPF) and transient stability constraint generation slave subproblems, afterward the master and slave problems were solved alternately. In [5], the transient stability constraint was formulated in terms of steady-state variables and embedded into a conventional OPF problem; then an active power re-dispatch sequential approach was followed to solve TSCOPF.

A numerical discretization method was applied to discretize the original TSCOPF into a large-scale nonlinear programming problem and then solve it by classical optimization algorithms such as the interior point method (IPM) [6]. In [7], an infinity norm was introduced to transform the infinite constraints into finite constraints. Next, the Jacobian and Hessian matrices of the transformed model were calculated to solve TSCOPF. In [8], a numerical discretization method enhanced by substituting DAE equalities with inequalities was presented to improve TSCOPF optimization efficiency. In [9], a single machine equivalent (SIME) theory was introduced to transform the initial multi-machine transient stability constraints into a one-machine angle constraint. However, an enormous amount of transient stability solutions was still required for the entire time-domain simulation period. In [10], a SIME-based TSCOPF method was designed to reduce the number of constraints. As a result, the Jacobian and Hessian matrices only required to be derived during a short unstable time period. As an enhancement of [10], an improved SIME method was proposed in [11] to reduce the stability constraints largely into one single SIME angle constraint by using a linear extrapolation or interpolation of two successive iterations.

The third method to solve TSCOPF is based on AI-related algorithms such as differential evolution algorithm [12], particle swarm optimization (PSO) [13], and group search optimization [14]. They mimic the natural intelligence of a specific biology to perceive its environment for achieving established goals. A self-adaptive differential evolution algorithm was employed in [12] to eliminate the strategy selection. An effective approach was thus formed to solve discrete non-differentiable TSCOPF. In [13], a data mining technique was first introduced to estimate the transient stability region. Then, a chaotic PSO algorithm combined with a two-stage support vector machine was proposed to solve TSCOPF. The generation valve-point effects and prohibited operation zones were considered in [14] to refine the TSCOPF model. Then, a hybrid group search optimization algorithm comprising a backward searching strategy, Cauchy mutation, and an inheritance operator was employed to solve discontinuous non-convex TSCOPF. Although AI methods are direct and powerful to address continuous and discrete control variables, they are usually non-deterministic and time-consuming. Therefore, some hybrid TSCOPF approaches are accordingly applied to leverage the advantages of both AI and derivative-based methods [15],[16].

Indeed, the aforementioned approaches made significant contributions to the solution of TSCOPF with a focus on driving normal unstable power systems back into stable conditions. However, the alleviation of extremely unstable

This work was supported partially by The Smart Grid Joint Foundation Program of National Natural Science Foundation of China and State Grid Corporation of China (U1866204), the Jiangsu Basic Research Project (Natural Science Foundation BK20180284), and the Fundamental Research Funds for the Central Universities (2019MS007). S. Xia, Z. Ding and G. Li are with the State Key Laboratory of Alternate Electrical Power System with Renewable Energy Sources, North China Electric Power University, Beijing 102206, China (s.w.xia@ncepu.edu.cn; zhaohao.ding@ncepu.edu.cn; ligy@ncepu.edu.cn). M. Shahidehpour is with Illinois Institute of Technology, Chicago, IL 60616 USA (ms@iit.edu). He is also a Research Professor with the Center of Research Excellence in Renewable Energy and Power Systems, King Abdulaziz University, Jeddah, Saudi Arabia. K.W. Chan and S. Bu with the Department of Electrical Engineering, The Hong Kong Polytechnic University, Hong Kong (eekwchan@polyu.edu.hk; siqi.bu@ polyu.edu.hk).

power systems, which are set apart from normal unstable cases, and driving them economically into stable conditions have not been fully addressed. Therefore, in this paper, an energy-based transient stability index is defined for extremely unstable conditions as a first step, and a unified energy-based transient stability constraint is established for both normal and extremely unstable TSCOPF. Next, the generalized TSCOPF is solved by iteratively addressing OPF and conducting the calculation of trajectory sensitivity. Furthermore, the accuracy-based perturbation technique is refined to address issues related to over-stabilized systems. Finally, two case studies are simulated to check the effectiveness of the proposed approach.

The main contributions of this paper are threefold:

1) Distinguished from [18], a novel energy-based transient stability index is specially defined for extremely unstable power systems, which forms a unified TSCOPF model for both normal and extremely unstable conditions.

2) Considering the unified transient stability constraint and the accuracy-based perturbation technique, a stability margin controllable TSCOPF approach is proposed which can effectively maintain a power system transient stability margin and its economic operation simultaneously.

3) By utilizing the parallelized TSCOPF divide-and-conquer approach, the detailed simulation results of two case studies have validated the effectiveness of the proposed approach for solving the TSCOPF problem with multiple extremely unstable contingencies.

The rest of this paper is organized as follows. The standard TSCOPF problem is reviewed in Section II. The energy-based transient stability constraint under extremely unstable conditions and the proposed TSCOPF approach are presented in Section III. Two case studies with multiple extremely unstable contingencies are tested in Section IV. Conclusions are presented in the last section.

II. Formulation of the TSCOPF Problem

The proposed TSCOPF model aims to design pre-contingency measures to stabilize harmful contingencies for preventive control, while considering the economic operation simultaneously [9]-[16]. The approach minimizes generator fuel costs by generation shift and the inclusion of static and dynamic security constraints. The proposed model is described as follows.

A. Objective Function

The TSCOPF objective is usually modeled by the generator fuel costs in a quadratic form as follows:

$$F_G = \sum_{i=1}^{n_G} a_i + b_i P_{Gi} + c_i P_{Gi}^2 \tag{1}$$

where n_G is the number of generators; P_{Gi} is the active power output of generator i; and a_i, b_i, and c_i are fuel cost coefficients.

B. Static Constraints

TSCOPF static constraints include active and reactive power balance equalities as well as pre-fault static security inequalities as follows:

1) Active and reactive power balance constraints:

$$\begin{cases} 0 = P_{Gi} - P_{Di} - V_i \sum_{j=1}^{n_b} V_j (G_{ij}\cos\theta_{ij} + B_{ij}\sin\theta_{ij}) \\ 0 = \mathrm{Q}_{Gi} - Q_{Di} - V_i \sum_{j=1}^{n_b} V_j (G_{ij}\sin\theta_{ij} - B_{ij}\cos\theta_{ij}) \end{cases} (i = 1,2,...,n_b) \tag{2}$$

where n_b is the total number of buses; P_{Di} and Q_{Di} are the active and reactive load demands; Q_{Gi} is the i^{th} generator reactive power; V_i is the voltage magnitude of bus i ; and θ_{ij} is the angle difference between nodes i and j.

2) Static inequality constraints during pre-fault:

$$P_{Gi\min} \le P_{Gi} \le P_{Gi\max} (i = 1,2,.....,n_G) \tag{3}$$

$$Q_{Gi\min} \le Q_{ri} \le Q_{Gi\max} (i = 1,2,.....,n_G) \tag{4}$$

$$V_{i\min} \le V_i \le V_{i\max} (i = 1,2,.....,n_b) \tag{5}$$

$$S_{l\min} \le S_l \le S_{l\max} (i = 1,2,.....n_l) \tag{6}$$

where n_l is the total number of branches. Eqs. (3) and (4) represent the active/reactive power limits of generator i; Eq. (5) denotes the upper and lower limits of the voltage magnitude of bus i; Eq. (6) stands for the thermal limits of transmission line l.

C. Dynamic constraints during fault and post-fault

Dynamic constraints during fault and post-fault are stated by DAEs as follows:

$$\begin{cases} \dot{x} = f(x(t), y(t), \alpha), x(t_0) = x_0 \\ 0 = g(x(t), y(t), \alpha), y(t_0) = y_0 \end{cases} \tag{7}$$

where x and y are the vector of state variables and algebraic variables, respectively, and α represents the control variables. DAEs in (7) can be easily solved by the implicit trapezoidal integration algorithm in a time-domain simulation.

SIME is a powerful hybrid method for multi-machine transient stability analyses [17],[18]. SIME performs the conventional time domain (TD) simulation by solving the differential-algebraic equations to determine the separation mode of multiple machines into Critical Machines (CMs) vs Non-critical Machines (NMs), which are finally mapped into a one-machine infinite-bus (OMIB) equivalent to calculate the transient stability margin via the extended equal area criterion. To correctly identify CMs and NMs, SIME applies the TD program in during-fault and post-fault periods. At each time step of the TD program, SIME sorts out the machines according to their rotor angles, and several separation patterns of the two machine-angle clusters are constructed based on the rotor angle deviations between adjacent machines' rotor trajectories (e.g., top 3 largest angle deviations) [4], [18]. Each candidate for the clustering of machines is replaced by OMIB, and the candidate OMIB that has the lowest stability margin is declared as the designated cluster.

Based on OMIB, the original multi-machine system expressed by (7) can be mapped as

$$\begin{cases} M_E \dfrac{d\omega_E}{dt} = P_{mE} - P_{eE} = P_a \\ \dfrac{d\delta_E}{dt} = \omega_E \end{cases} \tag{8}$$

where $M_E = M_C M_N/(M_C + M_N)$ is the equivalent SIME inertial, with $M_C = \sum_{i\in C} M_i$ and $M_N = \sum_{j\in N} M_j$; subscripts C and N stand for CMs and NMs, respectively; $P_{mE} = M_E(M_C^{-1}\sum_{i\in C} P_{Gi} - M_N^{-1}\sum_{j\in N} P_{Gj})$ and $P_{eE} = M_E(M_C^{-1}\sum_{i\in C} P_{ei} - M_N^{-1}\sum_{j\in N} P_{ej})$ are the SIME mechanical and electric power, respectively; $\delta_E = \delta_C - \delta_N = M_C^{-1}\sum_{i\in C} M_i\delta_i - M_N^{-1}\sum_{j\in N} M_j\delta_j$, and $\omega_E = \omega_C - \omega_N = M_C^{-1}\sum_{i\in C} M_i\omega_i - M_N^{-1}\sum_{j\in N} M_j\omega_j$ are the equivalent SIME angle and speed; and δ_i, ω_i, M_i, P_{Gi}, P_{ei} (δ_j, ω_j, M_j, P_{mj}, P_{ej}) are the generator angle, speed, time constant, mechanical and electric power of unit i for the original power system, respectively. And P_a is the accelerating power (i.e., mechanical-electric power difference).

At each time step of the TD program, SIME sorts the machines out according to their rotor angles to generate the candidate OMIB; meanwhile SIME also check the settled condition for identifying the normal unstable condition based on the candidate OMIB. The system is defined as normal unstable when the following condition is satisfied,

$$\begin{cases} P_a(t_u) = P_{mE}(t_u) - P_{eE}(t_u) = 0 \\ \dot{P}_a(t_u) = \dfrac{dP_a}{dt} > 0 \end{cases} \quad (9)$$

where t_u is the time at the exit point when (9) holds, and the stability margin is quantified by,

$$\eta_u = -\frac{1}{2} M_E (\omega_E(t_u))^2 \quad (10)$$

where η_u represents the residual kinetic energy at the exit point when the potential energy is offset by the kinetic energy at t_u.

For a stable system, before approaching the exit point, the system stops its excursion at δ_r (maximum angle excursion) and t_r, where the following condition is satisfied:

$$\begin{cases} \omega(t_r) = 0 \\ P_a(t_r) = P_{mE}(t_r) - P_{eE}(t_r) < 0 \end{cases} \quad (11)$$

The stability margin is approximated according to the linearized trajectory of p_a as follows:

$$\eta_s = |P_a(t_r)|(\delta_u - \delta_r)/2 \quad (12)$$

where δ_u is the angle when the generator active power is the same as the mechanical power, calculated by the second-kick method [19]; $P_a(t_r)$ is the accelerating power) at δ_r.

For an extremely unstable system, P_{mE} will remain larger than P_{eE} even after a fault is cleared and there is no intersection of P_{mE} and P_{eE} [17],[18]. Based on this observation, a system is defined extremely unstable if the condition (13) is satisfied according to the SIME theory [17],[18],

$$P_a(t) = P_{mE}(t) - P_{eE}(t) > 0, \forall t > t_{cl} \quad (13)$$

When comparing the definition of (9) and (13), we have the following remarks: for the extremely unstable system, the mechanical power P_{mE} remains larger than electrical power P_{eE} after the fault is removed, and Eq. (13) indicates there is no intersection of P_{mE} and P_{eE}. (Please refer to the dark red line in Figures 1 or 2). However for the normal unstable system, the curve P_{eE} crosses P_{mE} and there is the intersection of P_{mE} and P_{eE}, or equivalently the accelerating power $P_a(t)=P_{mE}(t)-P_{eE}(t)$ passes by zero and continues increasing at t_u according to (9).

For extremely unstable conditions, the minimum accelerating power (14) is used to define the stability margin in [17], [18] as,

$$\eta_u = -P_{a\min}(t_{\min}) = -\min\{P_a(t) = P_{mE}(t) - P_{eE}(t) > 0, \forall t > t_{cl}\} \quad (14)$$

where t_{cl} is the fault clearing time and t_{min} is the moment at which the accelerating power reached its minimum after fault clearance.

The stability margin stated in (14) is not directly comparable to those in (10) or (12) given that the former is defined in terms of accelerating power while the latter two are defined from an energy perspective. To keep consistency with normal unstable and stable cases, we propose an energy-based stability margin in (15) for extremely unstable conditions and establish in Section III a unified energy-based transient stability constraint for the solution of both unstable and extremely unstable TSCOPF,

$$\eta_u = -\frac{1}{2} M_E (\omega_E(t_{cl}))^2 \quad (15)$$

It is noted that (15) merely represents the system kinetic energy accumulated during the fault period which is consistent with the definition of normal unstable or stable margin from an energy point of view. Furthermore, the proposed index (15) has the continuity property at the zero value. When (15) is larger than zero, the accelerating area is negative at the fault clearing time t_{cl}, and thereby an intersection of mechanical and electrical power occurs is ensured (as indicated by the pink shadow areas in Figs. 1(b) and 2(b)). In the next section, the rationale for using (15) in TSCOPF and its sensitivity calculations will be investigated for driving power systems from extremely unstable conditions back into stable conditions.

III. Proposed Stability Constrained TSCOPF Approach

In this section, the energy-based transient stability constraint is discussed and the proposed TSCOPF solution approach is presented.

A. Stability Constraints for Extremely Unstable TSCOPF

According to the stability margin under extremely unstable conditions defined by (14) in [17], [18], the criterion $\eta_u > 0$ should be satisfied so as to generate an intersection between P_{mE} and P_{eE} and drive an extremely unstable system to a normal stable condition. Assume that the stability margin at the k^{th} iteration in an extremely unstable condition which is stated as $\eta_u^k = -P_{a\min}^k$. Based on the linearization of (14), the transient stability constraint can be obtained as (16) to satisfy $\eta_u > 0$ at the $(k+1)^{\text{th}}$ iteration,

$$\eta_{new}^{k+1} = \eta_u^k + \sum_{i=1}^{n} \frac{d\eta_u^k}{dP_{Gi}^k} \Delta P_{Gi} > 0 \text{ or } P_{a\min}^k + \sum_{i=1}^{n} \frac{dP_{a\min}^k}{dP_{Gi}^k} \Delta P_{Gi} < 0 \quad (16)$$

where k is the iteration number, $\Delta P_{Gi}=P_{Gi}-P_{Gi}^k$, P_{Gi}, and P_{Gi}^k are the targeted power outputs in the $(k+1)^{\text{th}}$ iteration and the solution in the k^{th} iteration, respectively; $dP_{a\min}^k / dP_{Gi}^k$ denotes the sensitivity of the accelerating power to the power output of generator i at time $t_{\min}$. From (14), the stability margin in an extremely unstable condition is measured by the minimal of accelerating power $P_{a\min}$ as indicated by the mechanical-electric power difference on the dark red line in Figs. 1(a) and 2(a), and (16) would drive the system to a normal unstable condition represented by an intersection of mechanical and electrical power indicated by the pink line in Figs. 1(a) and 2(a). The two figures describe the relations of SIME accelerating power and angle in extremely unstable conditions with and without a peak at fault clearing moment t_{cl}.

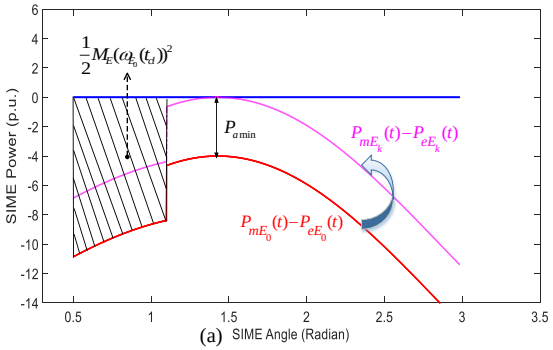

(a)

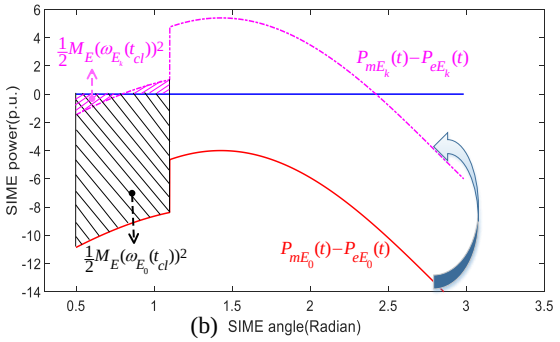

Fig. 1. SIME generator angle and power output with a peak not at t_{cl}.

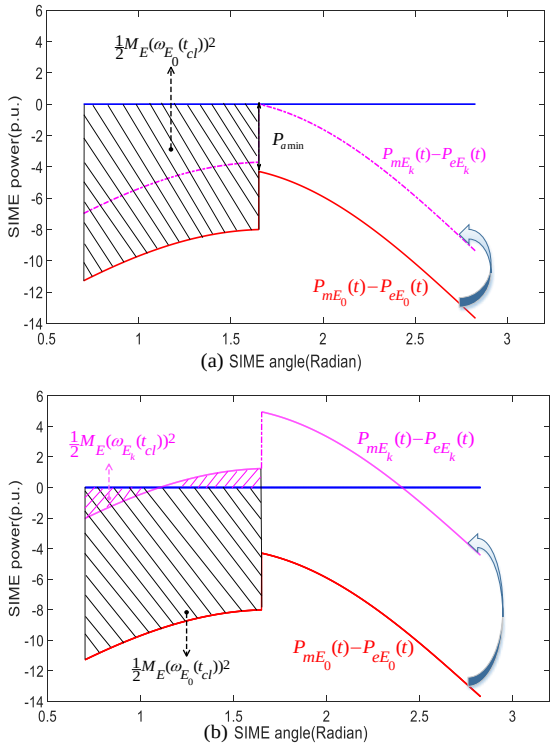

Fig. 2. SIME generator angle and power output with a peak at t_{cl}.

For the redefined stability margin in (15) under extremely unstable condition, denote the stability margin at the k^{th} iteration as $\eta_u^k = -\frac{1}{2}M_E^k(\omega_E^k(t_{cl}))^2$. The stability constraint is obtained by linearizing (15) at the k^{th} iteration to satisfy $\eta_u > 0$ for the $(k+1)^{\text{th}}$ iteration, which can drive the extremely unstable system back to a normal unstable condition. The resulted constraint is

$$\eta_{new}^{k+1} = \eta_u^k + \sum_{i=1}^{n}\frac{d\eta_u^k}{dP_{Gi}^k}\Delta P_{Gi} = \eta_u^k - M_E^k\sum_{i=1}^{n}[\omega_E^k(t_{cl})\frac{d\omega_E^k(t_{cl})}{dP_{Gi}^k}]\Delta P_{Gi} > 0 \quad (17)$$

where $d\omega_E^k(t_{cl})/dP_{Gi}^k$ is the SIME generator speed sensitivity to the power output of generator i at time t_{cl} at the k^{th} iteration.

The constraint in (17) derived from (15) can effectively drive the extremely unstable system back to a normal unstable condition. The rationale is as follows: the minimum kinetic energy at the fault clearing time t_{cl} in (15) stands for the accumulated energy during the fault period, as demonstrated by the black shadow area in Figs. 1(b) and 2(b). The constraint in (17) aims at decreasing the accelerating area to zero, thereby driving the system to the condition at which an intersection of mechanical and electrical power occurs, as indicated by the pink shadow area in Figs. 1(b) and 2(b). In this manner, the severity of extremely unstable condition will be alleviated, and the system will be driven back to a normal unstable condition. Comparing Fig. 1(a) and 1(b) or Fig. 2(a) and 2(b), it is obvious that (17) could more easily drive the extremely unstable system back to normal unstable condition than (16).

According to the margin definition in (10) in normal unstable condition and (15) in extremely unstable condition, the stability constraint stated in (17) could be unified and established for both normal and extremely unstable TSCOPF solutions based on the k^{th} iteration as follows:

$$\eta_{new}^{k+1} = \eta_u^k - M_E^k\sum_{i=1}^{n}[\omega_E^k(t_z)\frac{d\omega_E^k(t_z)}{dP_{Gi}^k}]\Delta P_{Gi} > 0 \quad (18)$$

where t_z is the exit time moment t_u for normal unstable condition or the fault clearing time t_{cl} for extremely unstable condition.

B. Proposed Accuracy-based Perturbation Strategy

The solution of TSCOPF may result in an over-stabilized power system; that is, the transient stability margin η_s may exceed a pre-defined stability margin tolerance η_t, i.e., $\eta_s > \eta_t$. To address this issue, an accuracy-based perturbation strategy is proposed to drive the system gradually from unstable condition into stable condition without becoming over-stabilized. The implementation details are as follows: if the power system is unstable in the k^{th} iteration but over-stabilized in the $k+1^{\text{th}}$ iteration, we reduce its stability margin η_u^k slightly by a factor of λ_j in (18). Accordingly, the unstable operation point will gradually shift across the stability boundary. Finally, a non-overstabilized condition will be established as follows:

$$\eta_{new}^{k+1} = \lambda_j\eta_u^k - M_E^k\sum_{i=1}^{n}[\omega_E^k(t_z)\frac{d\omega_E^k(t_z)}{dP_{Gi}^k}]\Delta P_{Gi} > 0 \quad (19)$$

where λ_j is updated by $\lambda_j = 0.5\lambda_{j-1}$ with $\lambda_0 = 1$ and j is the index of system over-stabilized based on the solution in k^{th} iteration. By gradually controlling the stability margin η_u^k using the factor λ_j, an unstable system will be gently driven back into a stable operation point without becoming over-stabilized. However, whether a power system is over-stabilized is an intuitive concept that depends on stability requirements of different systems. In this study, the tolerance η_t was set to 0.1 pu-rad [11]; that is, when the stability margin is larger than 0.1 pu-rad, the system is deemed over-stabilized and (19) is applied.

C. Trajectory Sensitivities Calculation of $d\omega_E/dP_{Gi}$

According to SIME, the sensitivities $d\omega_E/dP_{Gi}$ in (19) are a function of $d\omega_k/dP_{Gi}$ as follows:

$$\frac{d\omega_E^k(t_z)}{dP_{Gi}^k} = M_C^{-1}\sum\nolimits_{h\in C}M_h\frac{d\omega_h^k(t_z)}{dP_{Gi}^k} - M_N^{-1}\sum\nolimits_{j\in N}M_j\frac{d\omega_j^k(t_z)}{dP_{Gi}^k} \quad (20)$$

where $\frac{d\omega_h^k(t_z)}{dP_{Gi}^k}$ and $\frac{d\omega_j^k(t_z)}{dP_{Gi}^k}$ are the generator speed sensitivities of units h and j to the power output of unit i at time t_z, which is calculated by deriving the α sensitivity of (7) [20],

$$\begin{bmatrix} I-\frac{\Delta t}{2}f_x(x^t,y^t,\alpha) & -\frac{\Delta t}{2}f_y(x^t,y^t,\alpha) \\ g_x(x^t,y^t,\alpha) & g_y(x^t,y^t,\alpha)\end{bmatrix}\begin{bmatrix}x_\alpha^t \\ y_\alpha^t\end{bmatrix} = \begin{bmatrix}A^{t-1}+\frac{\Delta t}{2}f_\alpha(x^t,y^t,\alpha) \\ -g_\alpha(x^t,y^t,\alpha)\end{bmatrix} \quad (21)$$

where Δt is the integration time step; I is the identity matrix; $f_x(x^t,y^t,\alpha)=\partial f(x^t,y^t,\alpha)/\partial x^t$, $f_y(x^t,y^t,\alpha)=\partial f(x^t,y^t,\alpha)/\partial y^t$, $f_\alpha(x^t,y^t,\alpha)=\partial f(x^t,y^t,\alpha)/\partial \alpha$, $g_x(x,y,\alpha)=\partial g(x^t,y^t,\alpha)/\partial x^t$, $g_y(x,y,\alpha)=\partial g(x^t,y^t,\alpha)/\partial y^t$, $g_\alpha(x,y,\alpha)=\partial g(x^t,y^t,\alpha)/\partial \alpha$, and A^{t-1} only depends on the previous step t-1 as follows.

$$A^{t-1}=x_\alpha^{t-1}+\frac{\Delta t}{2}[f_x(x^{t-1},y^{t-1},\alpha)x_\alpha^{t-1} + f_y(x^{t-1},y^{t-1},\alpha)y_\alpha^{t-1}+f_\alpha(x^{t-1},y^{t-1},\alpha)] \quad (22)$$

The coefficient matrix on the left term of (21) is a by-product of solving (7) by the implicit trapezoidal integration algorithm in a time domain simulation; specifically, the calculation of (21) at each integration step is simply an extra Newton iteration of solving (7). Therefore, the trajectory sensitivities calculation of $d\omega_E/dP_{Gi}$ only slightly increases the computation burden of (7).

D. Proposed Parallel TSCOPF Approach

A divide-and-conquer approach is presented here to solve TSCOPF by decomposing it into a conventional OPF and transient stability constraint generation subproblems. The steps are presented as follows. 1) The SIME-based transient stability analysis and trajectory sensitivities calculation of $d\omega_E/dP_{Gi}$ are conducted in time-domain simulation for the OPF solution, then the transient stability constraints are generated from (19) and added to the OPF model in Step 2. 2) The OPF model with updated transient stability constraints derived from (19) is solved by IPM. 3) Steps 1 and 2 are solved iteratively until the power system solution is stable but non-overstabilized; that is the stability margin satisfies $\eta_t > \eta_s > 0$.

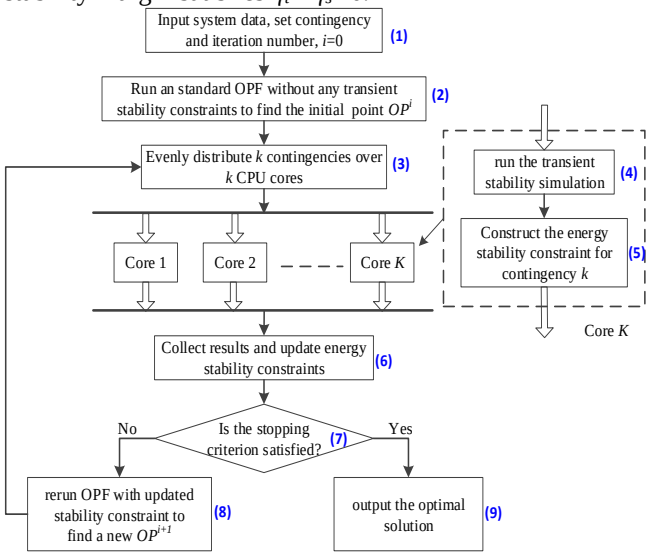

Fig. 3. Flowchart of the proposed parallelized TSCOPF algorithm.

The proposed TSCOPF model would be applied to an hour or half-hour ahead preventive control to simultaneously address the transient stability and economic issues. For practical applications, the computation efficiency of the proposed approach is enhanced in this paper. Consider that 1) the calculation burden of the proposed TSCOPF approach will linearly increase with the number of contingencies, and 2) the sensitivity calculation in (21) for each contingency can be done independently, and the solution of a multi-contingency constrained TSCOPF can be largely offset by applying a contingency-parallel calculation, as shown in Fig. 3, where k contingencies are farmed over k CPU cores for parallel transient stability analyses and trajectory sensitivity computations.

IV. Numerical Example

The effectiveness of the proposed TSCOPF approach was tested by the New England 10-generator and IEEE 50-generator systems. The transient stability time span was 5s. MATPOWER 4.1 [21] was adopted as the OPF engine, whereas the transient stability analysis and the trajectory sensitivity calculation were developed in-house with MATLAB R2016a on a PC with 3.2-GHz 6-core CPU and 8-GB RAM.

A. New England 10-generator 39-bus system

The New England 10-generator system was used as the first test-bed for validating the proposed approach. The network parameters were collected from [22] with generator fuel cost coefficients and ratings extracted from [9]. In the following, a single extremely unstable contingency and multi-contingency are respectively investigated.

1) Single extremely unstable contingency

A three-phase ground fault was applied at bus 29 at t=0s and subsequently cleared by tripping line 29-28 off after 0.35 s. First, the base OPF without any transient stability constraint is solved to obtain the starting point with a fuel cost of 60918.79 \$/h in Table I. The system is extremely unstable with G9 as CM and all other machines as NMs, as shown in Fig. 4(a). Given that no intersection exists for the SIME mechanical and electrical powers, the kinetic energy, i.e., -19.12 pu-rad, at the fault clearing time t_{cl} is deemed as the stability margin according to Eq. (15). The constraint expressed in (19) is then utilized to obtain an alleviated TSC-1 solution, as shown in Table I. The generator angle is depicted in Fig. 4(b). The system is normally unstable with a stability margin of -3.42 pu-rad. For the third iteration, this system exhibits a fuel cost of 62,586.46 \$/h, but it becomes over-stabilized with a stability margin of 0.39 pu-rad for a settled tolerance of 0.1 pu-rad. The corresponding generator angles are shown in Fig. 4(c). Based on the TSC-2 sensitivities and the constraint expressed in (19) with λ_j =0.5, a relaxed unstable solution is obtained as TSC-3 in Table I. The corresponding generator angles are shown in Fig. 4(d). After 4 iterations, the system evolves into stability with a fuel cost of 62,388.00 \$/h, as shown in TSC-4, and the generator angles presented in Fig. 4(e). At this point, the system is stable with a margin of 0.0126 pu-rad and non-overstabilized for a tolerance of 0.1 pu-rad. Comparing Figs. 4(e) with 4(c), we find that the maximal generator angle is increased from 138.2 to 157 degrees. This means that the proposed accuracy-based perturbation strategy indeed addresses the over-stabilized issue effectively.

When the stability margin defined in (14) [18] is used for the solution of TSCOPF, the optimal fuel cost becomes 62,405.08 \$/h and the stability margin is 0.036 pu-rad, which is obtained in 5 iterations, as shown in the last column of Table I. Compared with [18], the proposed approach achieves a comparable solution in fewer iterations. This is because the defined stability margin in (15) directly drives the system from extremely unstable condition into normal unstable condition in a single iteration, while the stability margin defined in (14) has to spend a few more iterations. These results imply that the proposed method is capable of achieving high-quality optimal solutions in a few iterations.

Table I. Solution of a single extremely unstable CTG-constrained TSCOPF.

Gen	Base OPF	Proposed method				[18]
		TSCOPF-1	TSCOPF-2	TSCOPF-3	TSCOPF-4	
G1	242.39	260.92	265.32	262.43	264.15	264.47
G2	566.94	611.70	650.00	615.35	623.19	622.48
G3	642.73	677.48	646.60	680.29	683.41	683.73
G4	629.5	670.76	714.01	674.10	678.21	678.39
G5	507.9	535.86	517.22	538.12	540.75	540.84
G6	650.38	690.66	748.29	693.92	697.96	698.09
G7	557.99	596.41	650.63	599.52	603.56	603.61
G8	534.76	575.82	554.42	579.19	582.16	582.68
G9	829.38	487.05	421.88	459.83	428.11	425.72
G10	977.57	1027.66	969.05	1031.71	1033.29	1034.8
Margin	-19.12	-3.42	0.39	-1.63	0.0126	0.036
Iterations	--	4				5
Cost ($/h)	60918	61985	62586	62162	62388	62405

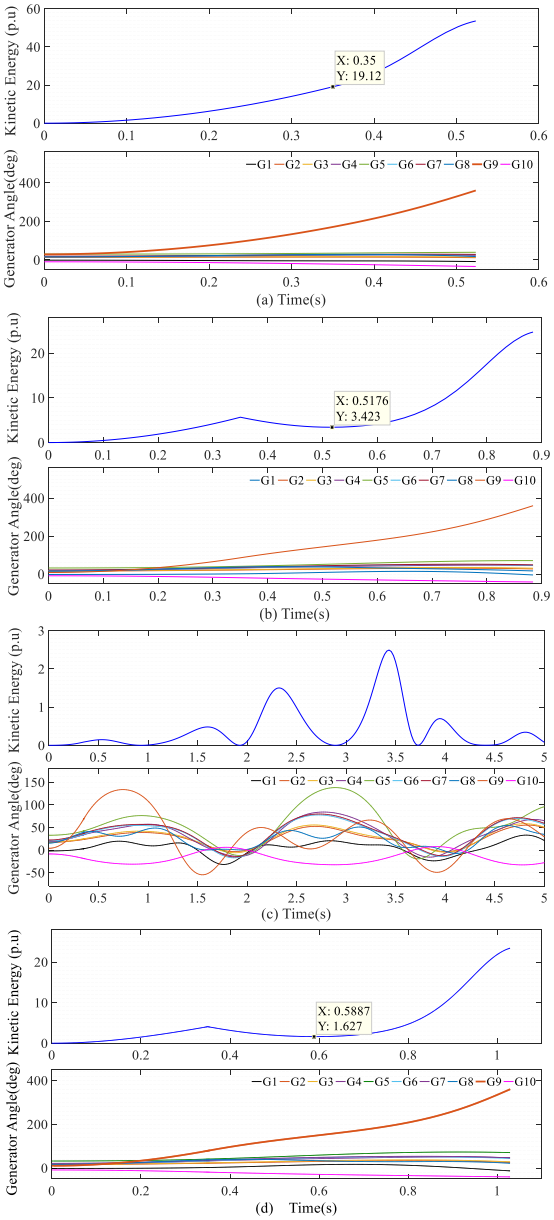

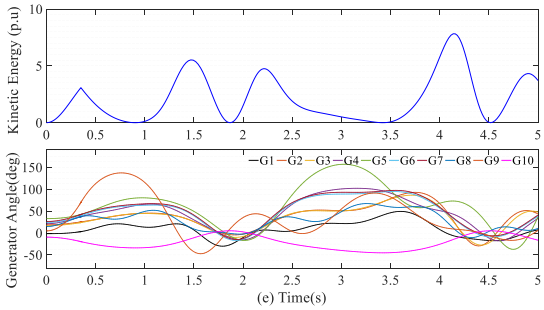

Fig. 4. Iterations of a single extreme unstable CTG-constrained TSCOPF.

2) Multiple extremely unstable contingencies

The next step is to evaluate the effectiveness of the proposed method for addressing multiple extremely unstable contingencies. The following two contingencies are considered:
CTG 1: a three-phase ground fault that occurs at bus 21 and is cleared after 0.16 s by tripping line 21–22.
CTG 2: a three-phase ground fault that occurs at bus 29 and is cleared after 0.35 s by tripping line 29–28.

These multiple contingencies take place with different SIME modes; that is, CTG 1 is normally unstable with G10 as NM and others as CMs, whereas CTG 2 is extremely unstable with G9 as CM and others as NMs. One stability constraint per contingency is constructed by using (19) at each iteration to search for a common stable operating point in both contingencies. After 2 iterations, the system becomes non-overstabilized for CTG 2 and unstable for CTG 1 with stability margins of 0.03 pu-rad and -0.2 pu-rad, respectively, while the fuel cost is 62,529.2 $/h, as shown in TSC-2 of Table II. Therefore, the stability constraint for CTG 2 remains unchanged according to TSC-1 while the constraint for CTG 1 is updated by (19) using TSC-2.

Table II. Solutions for CTG 1+2 constrained TSCOPF.

Gen	Base OPF	Proposed method for CTG A+B			[18]
		TSC-1	TSC-2	TSC-3	
G1	242.39	271.41	278.39	280.76	282.94
G2	566.94	633.21	649.98	641.63	644.63
G3	642.73	694.35	704.44	702.47	706.37
G4	629.50	674.93	677.87	669.54	674.39
G5	507.90	536.90	536.39	526.82	531.9
G6	650.38	646.43	628.11	632.33	631.04
G7	557.99	556.82	540.60	544.08	542.96
G8	534.76	592.33	603.83	605.31	610.58
G9	829.38	457.61	426.64	425.85	398.44
G10	977.57	1068.76	1086.08	1103.15	1109.05
Margin A	-0.97	-0.74	-0.20	0.55	0.0667
Margin B	-19.13	-1.80	0.03	0.05	0.2419
Iterations	--	3			4
Cost ($/h)	60918.79	62237.38	62529.20	62534.45	62756.8

Next, newly generated transient stability constraints for CTG 1 and CTG 2 are added to OPF and solved by IPM for the next optimal solution. The system is finally stabilized after 3 iterations with a fuel cost of 62,534.45 $/h and stability margins of 0.55 pu-rad and 0.05 pu-rad for CTG 1 and CTG 2, respectively. The full set of generator angles and kinetic energy for CTG 1 and CTG 2 are respectively depicted in Figs. 5(a-1) to (d-1) and (a-2) to (d-2) during the iterative procedures. For comparison, using the definition in [18], 4 iterations are required to reach the stable optimal solution with a fuel cost of 62,756.8 $/h, which means that more iterations are needed in [18] to obtain a comparable optimal solution with respect to the proposed approach. Compared with the single extremely unstable contingency in Table I, multi-contingency TSCOPF results represent a slightly more expensive case because more

transient stability constraints must be considered to find a common stable operation point.

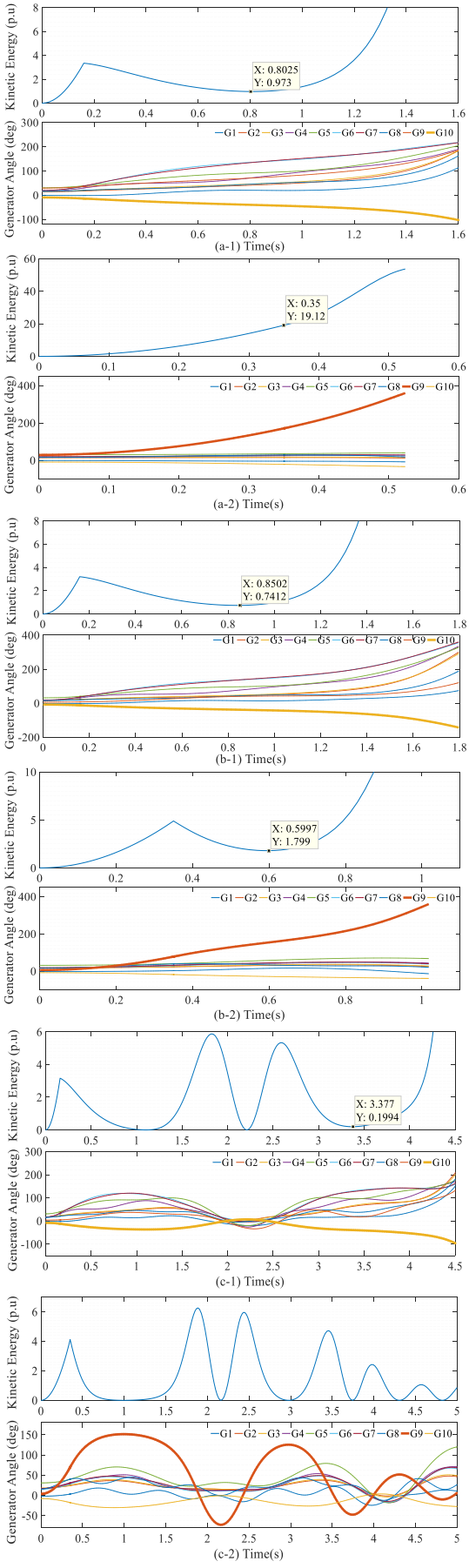

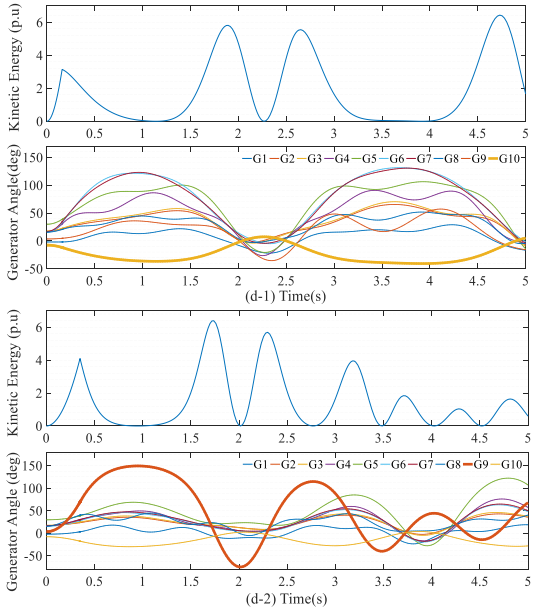

Fig. 5. Iterations of CTG 1+2 constrained TSCOPF in the New England system.

B. IEEE 50-generator 145-bus system

The IEEE 50-generator 145-bus system reported in [23] is adopted as a large system to evaluate the proposed approach under the following contingencies:

CTG 3: a three-phase ground fault near bus 89 is applied at t=0 and cleared by tripping line 89-103 off at 0.42s.

CTG 4: a three-phase ground fault occurs at bus 108 at t=0 and is cleared after 0.26s by tripping line 108–73 off.

Table III shows the multi-contingency 3+4 constrained TSCOPF solutions obtained by the proposed approach. The OPF without any transient stability constraint is first solved by IPM for the initial point, as showed in the second column of Table III. Although the fuel cost was quite low, i.e., 51,432,959.21 $/h, the system becomes extremely unstable, with stability margins of -10.25 pu-rad and -26.12 pu-rad for CTG 3 and CTG 4, respectively. Accordingly, the system kinetic energy and generator angles are presented in Figs. 6(a-1) and (a-2). Then, the transient stability constraint in (19) is derived and added as an extra constraint into OPF. Next, a new optimal point is calculated as TSC1 in Table III.

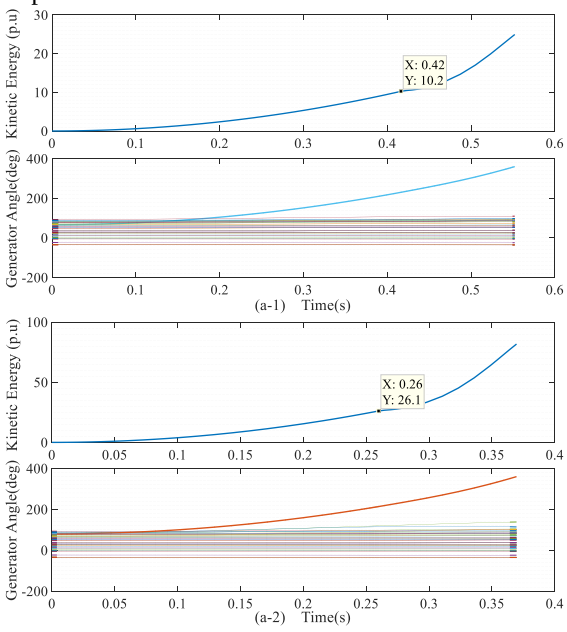

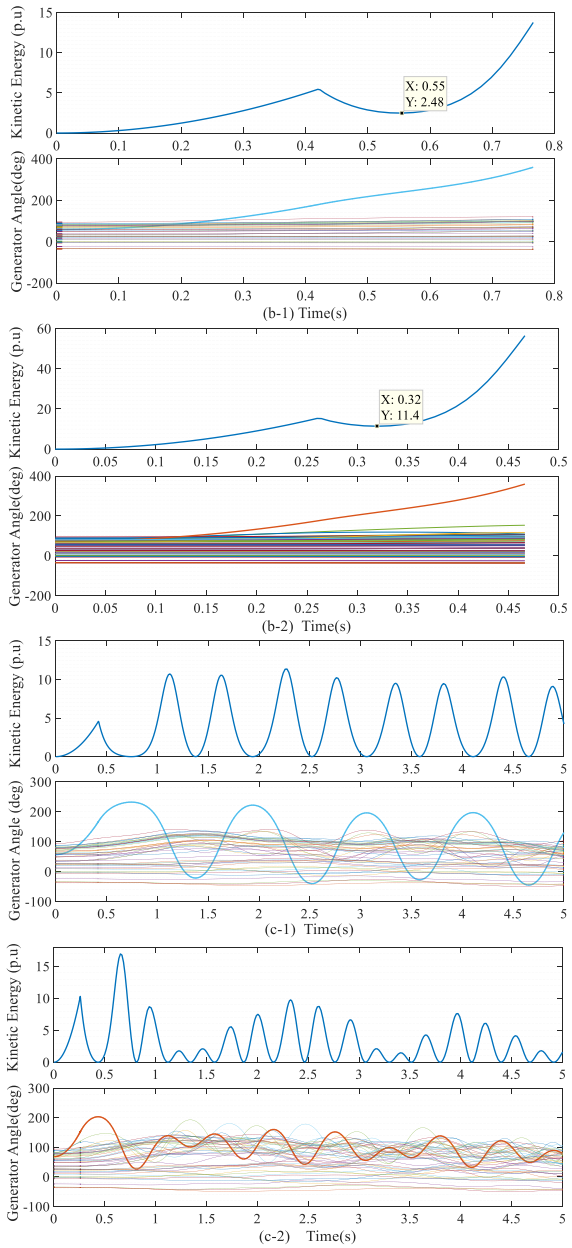

Fig. 6. Iterations of CTG 3+4 constrained TSCOPF for IEEE 50-gen system

Table III. Solutions of CTG 3+4 constrained TSCOPF for IEEE 50-gen system.

Gen No.	Base OPF (MW)	Proposed method (MW)		[18] (MW)
		TSC1	TSC2	
60	71.40	71.40	71.40	71.40
67	1480.80	1488.54	1494.53	1498.87
79	201.68	213.08	217.79	223.69
80	0.00	0.00	0.00	0.00
82	98.00	98.00	98.00	98.00
89	360.14	260.70	239.06	209.90
90	30.80	30.80	30.80	30.80
91	89.60	89.60	89.60	89.60
93	980.00	980.00	980.00	980.00
94	210.15	210.95	211.09	211.28
95	183.40	183.40	183.40	183.40
96	84.00	84.00	84.00	84.00
97	196.00	196.00	196.00	196.00
98	466.74	487.25	489.41	487.40
99	280.00	280.00	280.00	280.00
100	172.21	183.91	185.75	187.03
101	434.00	434.00	434.00	434.00
102	2505.14	2500.09	2501.84	2500.05
103	112.48	125.97	128.49	131.37
104	1267.68	1294.99	1302.89	1303.68
105	1365.05	1399.04	1412.64	1417.50
106	1282.95	1318.44	1329.92	1332.73
108	1120.00	857.47	704.66	682.90
109	72.80	72.80	72.80	72.80
110	980.00	980.00	980.00	980.00
111	1391.58	1414.84	1423.01	1424.87
112	420.00	420.00	420.00	420.00
115	3490.20	3490.20	3490.20	3490.20
116	3798.20	3798.20	3798.20	3798.20
117	2380.31	2377.69	2378.23	2382.23
118	5908.00	5908.00	5908.00	5908.00
119	12675.60	12675.60	12675.60	12675.60
121	3829.44	3968.02	4050.96	4067.87
122	1094.10	1094.22	1094.01	1094.14
124	2362.75	2368.26	2375.44	2382.31
128	14403.59	14498.22	14551.71	14554.68
130	8311.80	8311.80	8311.80	8311.80
131	19394.78	19378.94	19363.24	19363.51
132	4088.95	4073.89	4067.15	4066.55
134	17267.31	17285.08	17291.21	17292.97
135	7576.64	7575.98	7575.78	7575.51
136	43663.39	43657.02	43656.20	43654.55
137	14467.30	14467.30	14467.30	14467.30
139	48545.27	48541.91	48541.19	48540.54
140	27885.33	27885.33	27885.33	27885.33
141	31070.94	31078.95	31078.99	31081.84
142	21558.11	21523.70	21508.56	21507.63
143	7355.60	7355.60	7355.60	7355.60
144	15955.80	15955.80	15955.80	15955.80
145	15401.05	15387.36	15383.38	15381.49
Margin A	-10.25	-2.48	0.09	0.09
Margin B	-26.12	-11.39	0.71	1.05
Iterations	-----	2		3
Cost($/h)	51432959.21	51439055.15	51443343.50	51444589.38

At this point, the system normally becomes unstable for both CTG 3 and CTG 4, while the minimum kinetic energy is 2.48 pu-rad at 0.55s and 11.39 pu-rad at 0.32s, as shown in Figs. 6(b-1) and (b-2). This iterative procedure continues until the system becomes stable for both contingencies. The final fuel cost is 51,443,343.50 $/h, as given by TSC2. Meanwhile, the stability margins are 0.09 pu-rad and 0.71 pu-rad for CTG 3 and CTG 4, respectively. The system kinetic energy and generator angles are correspondingly depicted in Fig. 6(c-1) and (c-2). Moreover, when compared with the solution based on the transient stability margin defined in [18] (last column in Table III), the proposed approach reaches an economic operation in fewer iterations, which means that the proposed method can effectively ensure both power system transient stability and economic operations simultaneously.

C. Computation Time Analysis

In order to demonstrate advantages of the proposed approach and contingency-parallel strategy, Table IV presents the computation time and total number of iterations of the proposed approach and [18] to solve TSCOPF for the two systems. Both approaches are implemented on a PC with 3.2-GHz 6-core CPU and 8-GB RAM, but only different transient stability constraints for extremely unstable conditions are adopted, where (19) is used for the proposed approach vs (16) used for [18]. The total number of iterations and the computation time for the OPF solution and generating transient stability constraint (GTSC) are detailed in columns 4 and 5 of Table IV. In the table, the data in the last row are obtained with the multi-core contingency-parallel calculation, where one CPU is used to conduct the transient stability analysis and trajectory sensitivities calculation for one contingency (see step (3) in Fig. 3). The data in the first six rows are calculated without using the multi-core parallel processing strategy.

Table IV. Computation time for solving various TSCOPF problems

Systems	Method		Iterations	OPF+GTSC=Total Time (s)
New England 10-Gen	Single CTG	[18]	5	1.31+7.13=8.44
		Proposed	4	1.12+5.35=6.47
	CTG 1+2	[18]	4	1.02+13.32=14.34
		Proposed	3	0.93+10.63=11.56
IEEE 50-Gen CTG 3+4	[18]		3	3.32+57.61=60.93
	Proposed		2	2.74+39.95=42.69
	Proposed (parallel)		2	2.85+24.21=27.06

For the New England 10-generator system, 4 iterations and 6.47s are required by the proposed approach to solve the single CTG, whereas 5 iterations and 8.44s are needed in [18]. For CTG 1+2, 3 iterations and 11.56s are spent to find the optimal solutions by the proposed approach, while 4 iterations and 14.34s are needed in [18]. Compared with the single CTG, the time consumption of CTG 1+2 is slightly larger owing to the number of transient stability analysis procedures increasing from 1 to 2 per iteration.

For the IEEE 50-generator system, 3 iterations and 60.93s are required to solve CTG 3+4 constrained TSCOPF based on the stability margin defined in [18]. Comparatively, 2 iterations and 42.69s are needed by the proposed approach. With the help of the parallel contingency computing strategy, the execution time is reduced to 27.06s, which means a speedup factor of 1.58. These investigations demonstrate that the proposed method can efficiently solve TSCOPF at a reasonable computation time.

V. Conclusion

In this study, an energy-based transient stability index is defined for the extremely unstable condition, and a unified transient stability constraint is established for both normal and extremely unstable TSCOPF models. The proposed TSCOPF is solved by iteratively addressing the OPF and conducting SIME-based trajectory sensitivity analyses. The accuracy-based perturbation strategy combined with parallel technique are also implemented to enhance its performance. By applying extensive tests on the New England 10-generator and IEEE 50-generator systems, we draw the following conclusions: 1) the proposed energy-based transient stability index is effective for the modeling and the solution of the TSCOPF problem under extremely unstable conditions; 2) the entire TSCOPF approach can efficiently solve TSCOPF using the proposed accuracy-based perturbation strategy and parallel computation technique, and considering multiple/extremely unstable contingencies via few iterations but with satisfactory stability margin. For our future work, the proposed approach will be combined with the automatic generation control to form an on-line coordinated energy management strategy for practical power networks.

References

[1] S. Abhyankar, G. Geng, M. Anitescu, X. Wang, and V. Dinavahi, "Solution techniques for transient stability-constrained optimal power flow – Part I," *IET Gener. Transm. Distrib.*, vol. 11, no. 12, pp. 3177-3185, Aug. 2017.

[2] L. Tang and W. Sun, "An automated transient stability constrained optimal power flow based on trajectory sensitivity analysis," *IEEE Trans. Power Syst.*, vol. 32, no. 1, pp. 590-599, Jan. 2017.

[3] X. Tu, L. Dessaint, and H. Nguyen-Duc, "Transient stability constrained optimal power flow using independent dynamic simulation," *IET Gener. Transm. Distrib.*, vol. 7, no. 3, pp. 244-253, Mar. 2013.

[4] Y. Xu, J. Ma, Z. Y. Dong, and D. J. Hill, "Robust transient stability-constrained optimal power flow with uncertain dynamic loads," *IEEE Trans. Smart Grid*, vol. 8, no. 4, pp. 1911-1921, Jul. 2017.

[5] A. Pizano-Martínez, C. R. Fuerte-Esquivel, E. A. Zamora-Cárdenas, and J. M. Lozano-García, "Directional derivative-based transient stability-constrained optimal power flow," *IEEE Trans. Power Syst.*, vol. 32, no. 5, pp. 3415-3426, Sep. 2017.

[6] H. Xin, D. Gan, Z. Huang, K. Zhuang, and L. Cao, "Applications of stability-constrained optimal power flow in the East China system," *IEEE Trans. Power Syst.*, vol. 25, no. 3, pp. 1423-1433, Aug. 2010.

[7]. Y. Xia and K. W. Chan, "Dynamic constrained optimal power flow using semi-infinite programming," *IEEE Trans. Power Syst.*, vol. 21, no. 3, pp. 1455-1457, Aug. 2006.

[8]. Q. Jiang and Z. Huang, "An enhanced numerical discretization method for transient stability constrained optimal power flow," *IEEE Trans. Power Syst.*, vol. 25, no. 4, pp. 1790-1797, Nov. 2010.

[9] R. Zarate-Minano, T. Van Cutsem, F. Milano, and A. J. Conejo, "Securing transient stability using time-domain simulations within an optimal power flow," *IEEE Trans. Power Syst.*, vol. 25, no. 1, pp. 243-253, Feb. 2010.

[10] A. Pizano-Martianez, C. R. Fuerte-Esquivel, and D. Ruiz-Vega, "Global transient stability-constrained optimal power flow using an OMIB reference trajectory," *IEEE Trans. Power Syst.*, vol. 25, no. 1, pp. 392-403, Feb. 2010.

[11] A. Pizano-Martinez, C. R. Fuerte-Esquivel, and D. Ruiz-Vega, "A new practical approach to transient stability-constrained optimal power flow," *IEEE Trans. Power Syst.*, vol. 26, no. 3, pp. 1686-1696, Aug. 2011.

[12] Y. Chen, F. Luo, Y. Xu, and J. Qiu, "Self-adaptive differential approach for transient stability constrained optimal power flow," *IET Gener. Transm. Distrib.*, vol. 10, no. 15, pp. 3717-3726, Nov. 2016.

[13] Y. Zhou, J. Wu, L. Ji, Z. Yu, K. Lin, and L. Hao, "Transient stability preventive control of power systems using chaotic particle swarm optimization combined with two-stage support vector machine," *Electric Power Systems Research*, Vo. 155, pp. 111-120, Feb. 2018.

[14] S. Xia, B. Zhou, K. W. Chan, and Z. Guo. "An improved GSO method for discontinuous non-convex transient stability constrained optimal power flow with complex system model," *Int. J. Electr. Power Energy Syst.*, vol. 64, pp. 483-492, Jan. 2015.

[15] Y. Xu, Z. Y. Dong, K. Meng, J. H. Zhao, and K. P. Wong, "A hybrid method for transient stability-constrained optimal power flow computation," *IEEE Trans. Power Syst.*, vol. 27, no. 4, pp. 1769-1777, Nov. 2012.

[16] H. Ahmadi, H. Ghasemi, A.M. Haddadi, and H. Lesani, "Two approaches to transient stability-constrained optimal power flow," *Int. J. Electr. Power Energy Syst.*, vol. 47, pp. 181-192, May 2013.

[17] M. Pavella, D. Ernst, and D. Ruiz-Vega, *Transient stability of power systems: a unified approach to assessment and control*: Norwell, MA: Kluwer, 2000, pp. 33-64.

[18] D. Ernst, D. Ruiz-Vega, M. Pavella, P. M. Hirsch, and D. Sobajic, "A unified approach to transient stability contingency filtering, ranking and assessment," *IEEE Trans. Power Syst.*, vol. 16, no. 3, pp. 435-443, Aug. 2001.

[19] D. Fang, T. S. Chung, Y. Zhang, and W. Song, "Transient stability limit conditions analysis using a corrected transient energy function approach," *IEEE Trans. Power Syst.*, vol. 15, no. 2, pp. 804-810, May 2000.

[20] G. Hou and V. Vittal, "Cluster computing-based trajectory sensitivity analysis application to the WECC system," *IEEE Trans. Power Syst.*, vol. 27, no. 1, pp. 502-509, Feb. 2012.

[21] R. D. Zimmerman, C. E. Murillo-Sanchez, and R. J. Thomas, "MATPOWER: steady-state operations, planning, and analysis tools for power systems research and education," *IEEE Trans. Power Syst.*, vol. 26, no. 1, pp. 12-19, Feb. 2011.

[22] M. A. Pai, *Energy Function Analysis for Power System Stability*: Norwell, MA: Kluwer, 1989.

[23] A.A. Fouad and V. Vittal, *Power system transient stability analysis using the transient energy function method*: Englewood Cliffs, NJ, 1992.

Biographies

Shiwei Xia (S'11-M'15-SM'20) received the Ph.D. degree in power systems from The Hong Kong Polytechnic University, Hung Hom, Hong Kong, in 2015. Currently, he is with the State Key Laboratory of Alternate Electrical Power System with Renewable Energy Sources, School of Electrical and Electronic Engineering, North China Electric Power University, Beijing, China, and also a Visiting Faculty with the Robert W. Galvin Center for Electricity Innovation, Illinois Institute of Technology, Chicago, IL, USA. His research interests include security and risk analysis for power systems with renewables, distributed optimization and control of AC-DC distribution grid.

Zhaohao Ding (S'11–M'15) received the Ph.D. degree in electrical engineering from the University of Texas at Arlington, Arlington, TX, USA, in 2015. He is currently an Associate Professor with North China Electric Power University, Beijing, China, and a Research Member with Academy of Modern Electric Power Research. His areas of interest include power system planning and operation, power market and stochastic optimization.

Mohammad Shahidehpour (F'01) received the Honorary Doctorate degree in electrical engineering from the Polytechnic University of Bucharest, Bucharest, Romania. He is the Bodine Chair Professor and Director of the Robert W. Galvin Center for Electricity Innovation, Illinois Institute of Technology, Chicago, IL, USA. He is a Fellow of IEEE, Fellow of the American Association for the Advancement of Science (AAAS), and Fellow of the National Academy of Inventors (NAI). Dr. Shahidehpour is a member of the US National Academy of Engineering.

Ka Wing Chan (M'98) received the B.Sc. (with First Class Honors) and Ph.D. degrees in electronic and electrical engineering from the University of Bath, Bath, U.K., in 1988 and 1992, respectively. He currently is an Associate Head and Associate Professor in the Department of Electrical Engineering of The Hong Kong Polytechnic University. His general research interests include smart grid and renewable energy, power system stability analysis and control, power system planning and optimization, real-time power system simulation.

S. Q. Bu (S'11-M'12-SM'17) received the Ph.D. degree from the electric power and energy research cluster, The Queen's University of Belfast, Belfast, U.K., in 2012, where he continued his postdoctoral research work before entering industry. Subsequently, he joined National Grid UK as a Power System Engineer and then became an experienced UK National Transmission System Planner and Operator. He is an Assistant Professor with The Hong Kong Polytechnic University, Kowloon, Hong Kong, and also a Chartered Engineer with UK Engineering Council, London, U.K.. His research interests are power system stability analysis and operation control, including wind power generation, PEV, HVDC, FACTS, ESS and VSG.

Gengyin Li (M'03) received the Ph.D. degree in electrical engineering from North China Electricity Power University, Beijing, China, in 1996. He is currently a professor in the School of Electrical and Electronic Engineering, North China Electricity Power University. His research interests include HVDC transmission, power quality analysis and control, and new transmission and distribution technologies.